NUKLEONIKA 2005;50(2):73–81

ORIGINAL PAPER

Thermal and epithermal neutrons in the vicinity of the Primus Siemens biomedical accelerator

**Adam Konefał,
Marcin Dybek,
Wiktor Zipper,
Włodzimierz Łobodziec,
Katarzyna Szczucka**

Abstract In this paper, the thermal and epithermal neutron fluence distributions in the vicinity of the Primus Siemens accelerator are presented. The measurements were carried out by the use of the neutron activation method for 15 MV X-rays and electron beams of 18 MeV and 21 MeV. From the radiation safety point of view for the hospital personnel, it is important to know the thermal and epithermal neutron fluence distribution in the vicinity of the accelerator because the neutrons interacting with atoms of a medium by various processes induce the activity of objects (accelerator, other apparatus etc.) and walls in the treatment room. The thermal and epithermal neutron capture, particularly, in high atomic number materials of the accelerator head can be a significant source of gamma radiation and it has to be taken into account for estimation of the work safety of the personnel. Values of the neutron fluence were normalized to the maximum photon (or electron) dose $D_{\max,\gamma\,(e)}$ measured at the central axis of therapeutic X-ray (or electron) beam in a water phantom. The thermal neutron fluences measured during the 15 MV X-ray emission varied between 1.1×10^5 $n \cdot cm^{-2} \cdot Gy^{-1}$ and 4.4×10^5 $n \cdot cm^{-2} \cdot Gy^{-1}$ whereas the epithermal neutron fluences ranged from 0.2×10^5 $n \cdot cm^{-2} \cdot Gy^{-1}$ to 1.8×10^5 $n \cdot cm^{-2} \cdot Gy^{-1}$. In the case of electron beams, the neutron fluence measurements were performed only at the isocentre. The obtained thermal and epithermal neutron fluences were 1.2×10^4 $n \cdot cm^{-2} \cdot Gy^{-1}$ and 0.6×10^4 $n \cdot cm^{-2} \cdot Gy^{-1}$, respectively, for the 18 MeV electrons. In the the case of the 21 MeV electron beams the thermal neutron fluence was 2.0×10^4 $n \cdot cm^{-2} \cdot Gy^{-1}$ whereas the epithermal neutron fluence was 0.8×10^4 $n \cdot cm^{-2} \cdot Gy^{-1}$.

Key words biomedical accelerators • thermal neutrons • epithermal neutrons

A. Konefał✉, W. Zipper, K. Szczucka
Institute of Physics,
University of Silesia,
4 Uniwersytecka Str., 40-007 Katowice, Poland,
Tel.: +48 32/ 588 211(1384), Fax: +48 32/ 588 431,
E-mail: akonefal@uranos.cto.us.edu.pl

M. Dybek, W. Łobodziec
Radiotherapy Department of the Hospital – Memorial St. Leszczyński,
27 Raciborska Str., 40-074 Katowice, Poland

Received: 28 December 2004
Accepted: 25 April 2005

Introduction

In spite of the high progress that has been made in radiotherapy in the latter part of the 20th century, many problems still remain to be solved. One of them is the so-called neutron contamination, i.e. high-energy therapeutic beams, photon beams mainly, from biomedical accelerators are contamined with neutron radiation. Neutrons originate from photonuclear (γ,n) and electronuclear (e,e'n) reactions induced by photons and electrons of the therapeutic beam. The main source of these reactions is the accelerator head made of materials with high atomic numbers. The photonuclear reactions have a resonance character and the threshold energies of about 7–8 MeV. The theory of photonuclear reactions was reviewed by various authors (for example [6, 13, 14, 17, 18]). A comprehensive compilation of photonuclear reaction cross sections is included in Atomic Data and Nuclear Data Tables [2]. The electronuclear cross sections increase with electron energy [21] and the maximum probability of an electron interacting directly with a nucleus is about two orders of magnitude smaller than that of a photon in the range of energies of beams generated by biomedical accelerators.

The contaminant-neutrons have a broad energy spectrum with the high-energy end of several MeV [10,

19]. We have focused on the thermal and epithermal energy range. Knowledge of the thermal and epithermal neutron radiation level is important. The thermal and epithermal neutrons can induce activity in the treatment room because of a high probability for simple capture reaction (n,γ) for a number of nuclides. In the (n,γ) reactions, the stable isotopes change into radioisotopes with metastable states. The gamma rays from a deexcitation of these states are very penetrative i.e. they have even energies of several MeV. Moreover, electrons and alfa particles are emitted as a result of the radioactive-decay process. The radioisotopes can originate also directly from the photonuclear and electronuclear reactions. These two reactions and neutrons with thermal and epithermal energies are the main factors inducing radioactivity in the treatment room.

In this paper, the thermal and epithermal neutron fluence distributions in the vicinity of the Primus Siemens biomedical accelerators are presented. The obtained results were compared with that of analogous measurements for the Varian Clinac 2300 machines, shown in paper [11].

Measurements of neutron radiation are not easy to carry out in the vicinity of the biomedical accelerator because of a strong photon (or electron) flux. The fundamental requirement for these measurements is the use of a method capable to determine the neutron fluence independently of the photon flux value. An additional problem is the production of neutrons in the detector material. This production should be very low or easy to determine. We decided to use the neutron activation method for the thermal and epithermal neutron fluence measurements. The applied method fulfils the above mentioned conditions.

In addition, the gamma energy spectrum in the treatment room during the pause between the beam emissions was measured to get information about radioisotopes originating in the accelerator. Such information can be applied for the radiological protection of the personnel.

Material

Measurements were performed for two Primus Siemens accelerators installed in the Radiotherapy Department of the Hospital – Memorial St. Leszczyński in Katowice. The thermal and epithermal neutron fluence distributions were measured in four planes in the vicinity of the accelerator head (Fig. 1) during emission of a 15 MV X-ray beam and electron beams of 18 MeV and 21 MeV.

Resonance detectors made of indium foil (^{115}In isotope) were applied as neutron activation detectors in the neutron activation method. The indium foil detectors were shaped like a circle with a radius of 0.75 cm. The foil thickness was 100 μm (80 mg/cm^2). We decided to use the ^{115}In isotope because it has a relatively high cross section for thermal neutron capture (160 barns [1]) and a high resonance peak at 1.45 eV (about 28,000 barns [20]) and a number of lower resonances in the epithermal energy range, yielding the resonance activation integral of 2700 barns [15].

If the thermal or epithermal neutron hits the indium foil, then it can induce the following reaction:

$$(1) \qquad {}^{115}_{49}\mathrm{In} + {}^{1}_{0}\mathrm{n} \rightarrow {}^{116\mathrm{m}}_{49}\mathrm{In}\ (\text{metastable})$$

followed by the radioactive decay process:

$$(2) \qquad {}^{116\mathrm{m}}_{49}\mathrm{In}\left(T_{1/2} = 54.41\,\mathrm{min}\right) \xrightarrow[\beta^-]{} {}^{116}_{49}\mathrm{Sn}^{*} + \tilde{\nu}_e \rightarrow {}^{116}_{49}\mathrm{Sn} + \text{gammas}.$$

Measurement of the gamma spectrum from the decay of ^{116m}In was the basis for determining the activity of the indium foil detector. The spectral measurements were performed using a Ge(Li) detector connected to a multichannel analyser at the Institute of Physics of the Silesian University.

As mentioned above, the indium foil detector activity can be induced by thermal as well as epithermal neutrons. The cadmium cover method was applied to separate the activities due to each of these two groups of neutrons. In our measurements, the indium foil detector was sandwiched between cadmium sheets with a thickness of 1 mm. Cadmium absorbs almost all thermal neutrons, but lets through most of epithermal ones. Thus, the total activity in the indium foil detector covered by cadmium is induced by epithermal neutrons. However, some of epithermal neutrons are captured by the cadmium cover and it is necessary to introduce an appropriate correction factor allowing for this absorption effect. This correction factor, denoted as F_{Cd}, was equal to 1.14 [20] for the cadmium cover used in our measurements. In general, its value depends on the type and weight of the foil and also on the cadmium cover thickness.

The measurements of the gamma energy spectrum from the decays of the radioisotopes originated in the treatment room were carried out by the use of a high-purity Ge detector applied for the field spectrometry.

Method

Geometry of measurements

In measurements performed during emission of the 15 MV X-ray beam, the indium foil detectors were located in four planes in the vicinity of the accelerator head (Fig. 1). Neutron fluence for electron beams was only measured at the isocentre.

Course of measurements

At each location, shown in Fig. 1 the measurements were carried out two times using the detector with and without the cadmium cover. The total activity of the covered indium foil detector is induced by epithermal neutrons, whereas the difference between activities induced in the uncovered and covered detectors is the activity due to thermal neutrons. In each measurement, the indium foil detector was exposed to neutron radiation for 15 minutes. 4500 monitor units of the

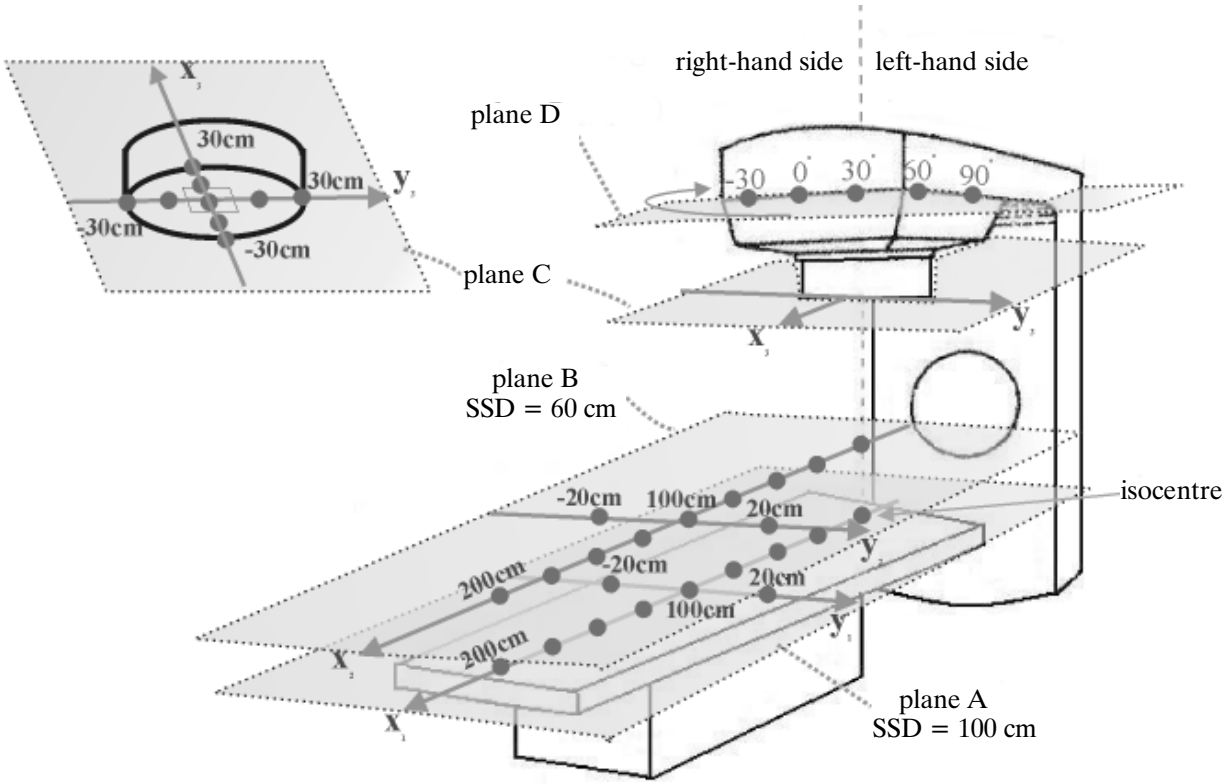

Fig. 1. Localizations of the indium foil detectors in the measurements carried out during emission of the 15 MV X-rays. The detector localizations are assigned with circles. The circles on the axes x_1, x_2 and y_1, y_2 correspond to the locations along and crosswise the treatment couch, respectively for SSD (source-skin distance) = 100 cm (plane A) and 60 cm (plane B). The plane C is located directly under the accelerator head. Moreover, the measurements were carried out on the front of the accelerator head casing (plane D).

therapeutic beam were emitted for this period of time. Afterwards, the excited indium foil detectors were removed from the treatment room to the Institute of Physics of Silesian University where the energy spectrum from the decay of the ^{116m}In state was measured for each detector. The activities of the indium foil detectors were determined by counting the gammas of 1294 keV. The gammas with other energies can be also used to determine the indium foil detector activities.

Relationship between the measured activity of the indium foil detector and fluence of neutrons hitting the foil

The detailed reason of the relationship between the measured indium foil detector activity and the neutron fluence was presented in the works which we refer to as [1, 11, 20] and in some others. In this paper we give the final formula for thermal neutrons:

$$\Phi_{ther} = \frac{A_{ther} W e^{\lambda t'}}{d_m S N_o \sigma_{ther} \left(1 - e^{-\lambda t_n}\right)} \tag{3}$$

and epithermal neutrons:

$$\Phi_{epi} = \frac{A_{epi} F_{Cd} W e^{\lambda t'}}{d_m S N_o C \left(1 - e^{-\lambda t_n}\right)} \int_{0.4eV}^{100keV} \frac{dE}{E} \tag{4}$$

where:

$$C = \int_{0.4eV}^{\infty} \frac{\sigma(E)}{E} dE \tag{5}$$

is the resonance activation integral.

Φ_{ther} – thermal neutron fluence; Φ_{epi} – epithermal neutron fluence; A_{ther} – measured indium foil detector activity due to neutrons; A_{epi} – measured indium foil detector activity due to epithermal neutrons; σ_{ther} – thermal neutron simple capture cross section; d_m – foil density (80 mg/cm^2); t_n – time of exposing to neutron radiation; t' – time between the end of the neutron exposure and the beginning of the measurement of the activity induced in the detector, i.e. the beginning of the measurement of the energy spectrum from the ^{116m}In state decay (shorter than half an hour); λ – decay constant (0.012739 min^{-1}); F_{Cd} – above-mentioned correction factor for absorption of epithermal neutrons in the cadmium sheets; W – atomic weight of material used as the neutron activation detector (^{115}In); S – foil area (1.767 cm^2); N_o – Avogadro's number.

Equations (3) and (4) do not include correction for self-shielding effects within the indium foil. As our test measurements performed by the use of the thiner indium foils have shown, this correction did not give a significant contribution to the neutron fluence values.

It is convenient to use the resonance activation integral because it makes calculation easier. Eq. (4) is

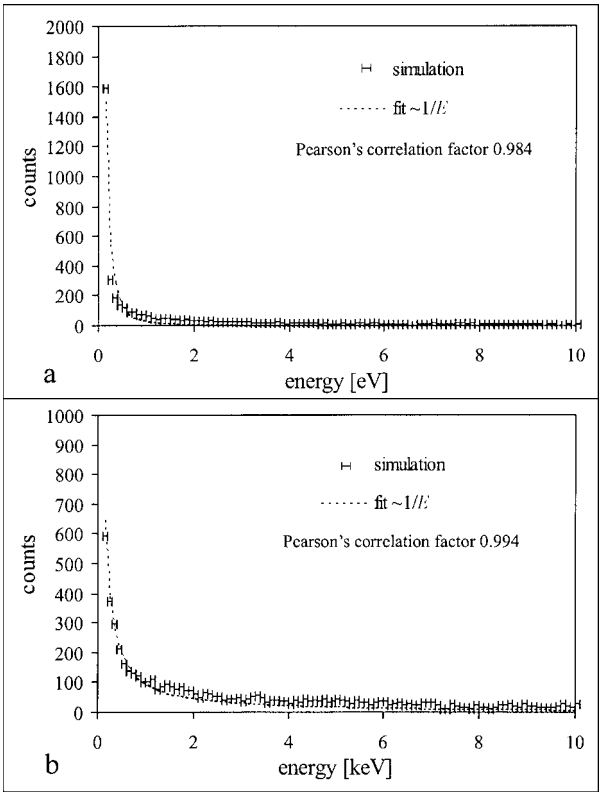

Fig. 2. The epithermal neutron spectra derived in plane A from the Monte Carlo simulation and the $1/E$ fit to the derived spectra. To obtain the spectra, the range of neutron energies was divided into intervals (bins) and the number of neutrons within each energy interval was counted. a – The neutron spectrum in the energy range from 0.1 eV to 10 eV (the energy intervals are 0.1 eV wide); b – the neutron spectrum ranging in energy from 0.1 keV – 10 keV (the energy intervals are 0.1 keV wide). Value of the Pearson's correlation factor close to 1 indicates that the spectrum has the character of $1/E$. The spectra in planes B, C and D (not presented in this paper) have also the $1/E$ character.

correct in the case when a number of neutrons is inversly proportional to their energy in the resonance energy range. As our Monte Carlo simulations have shown, such a situation occurs around the biomedical accelerator where large scattering processes take place (Fig. 2). The simulation program was written using the GEANT4 C++ libraries making it possible to simulate all important physical processes taking place in the accelerator head, in air and in walls during high-energy X-ray beam emission. These processes are:

- bremstrahlung production, ionization process, multiple scattering for electrons and positrons and additionally, positron anihilation, and
- photoelectric effect, compton interaction, gamma conversion, photonuclear reaction and Rayleigh scattering for photons, and some others of the lower significance, for example, the decay process etc.

The GEANT4 interaction models based on the G4EMLOW – version 2.3 and G4NDL3.7 data base were used to simulate the above-mentioned processes. The reliability of the GEANT4 calculations has been checked before by us and other authors (for example [3, 12]). However, we do not use simulations for the determination of the absolute values of neutron fluence because the data base with neutron process cross sections G4NDL3.7 did not include cross sections for some materials of minor components of the accelerator.

Correction (12%) of the decrease in the indium foil activity during the time of activity measurements was not specified in Eqs. (3) and (4) but it was taken into account. The results for the Varian Clinac accelerator, showed in paper [11] was not corrected for this decrease. However, we included this correction to all the presented thermal and epithermal neutron fluence values for more accurate comparison of the obtained results.

Values of neutron fluence were normalized to the maximum photon (or electron) dose $D_{\max,\gamma(e)}$ measured at the central axis of therapeutic X-ray (or electron) beam in a water phantom for given irradiation conditions determined by two parameters: radiation field size s and SSD. Such normalization made it possible to render the neutron fluence values independent of the accelerator efficiency. Fluence values measured in plane A were normalized to $D_{\max,\gamma}$ determined for s = 5 cm × 5 cm, 10 cm × 10 cm and 20 cm × 20 cm specified at SSD = 100 cm, whereas the values of fluences form measurements in plane B were normalized to $D_{\max,\gamma}$ determined for s = 6 cm × 6 cm specified at SSD = 60 cm. In the case of the remaining measurements, the normalization was carried out to $D_{\max,\gamma}$ determined for s = 10 cm × 10 cm specified at SSD = 100 cm.

A second order polynominal was fitted to all thermal and epithermal neutron fluence distributions shown in figures for better illustration of these distributions.

Results

Results for the 15 MV X-rays

The greater part of our measurements was performed during emission of the 15 MV X-ray beam because, as it was mentioned above, the probability of the photonuclear reactions is about two orders of magnitude greater than that of the electronuclear reactions for energies of the beams used in teleradiotherapy.

The thermal and epithermal neutron fluence distributions along the axes x_1 and y_1 (plane A) were measured for three radiation fields specified at SSD = 100 cm:

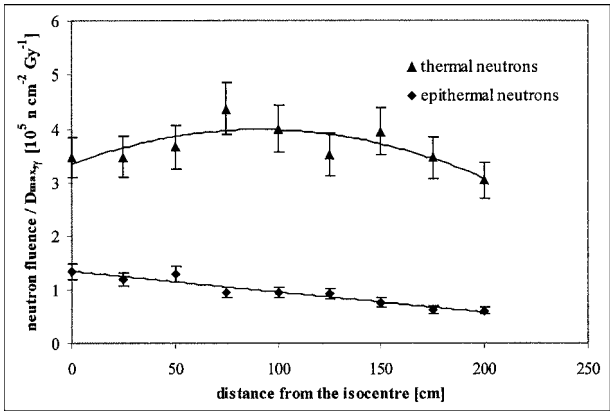

Fig. 3. The thermal and epithermal neutron fluence distributions along the axis x_1 for s = 5 cm × 5 cm specified at SSD = 100 cm.

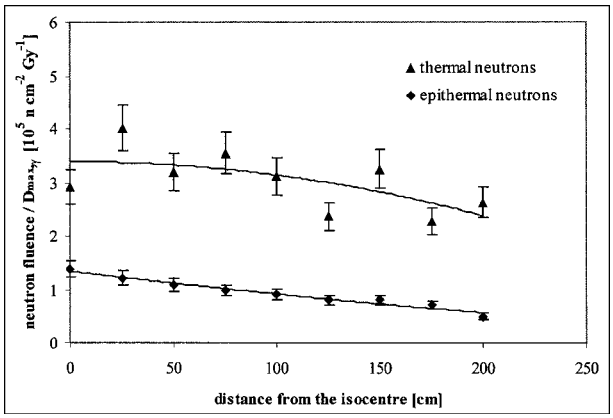

Fig. 4. The thermal and epithermal neutron fluence distributions along the axis x_1 for s = 10 cm × 10 cm specified at SSD = 100 cm.

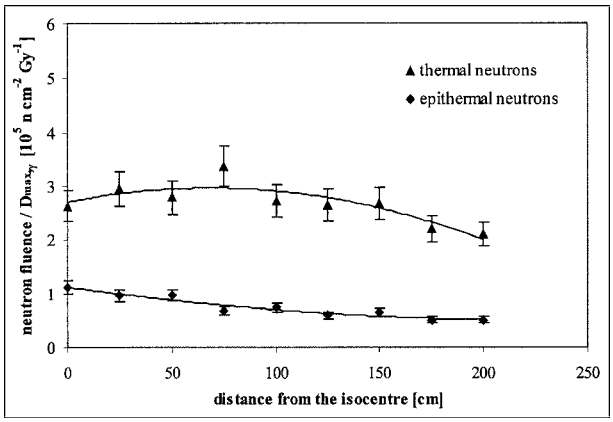

Fig. 5. The thermal and epithermal neutron fluence distributions along the axis x_1 for s = 20 cm × 20 cm specified at SSD = 100 cm.

s = 5 cm × 5 cm, 10 cm × 10 cm and 20 cm × 20 cm (Figs. 3, 4, 5 and Tables 1 and 2) whereas the measurements along the axes x_2 and y_2 were performed for the

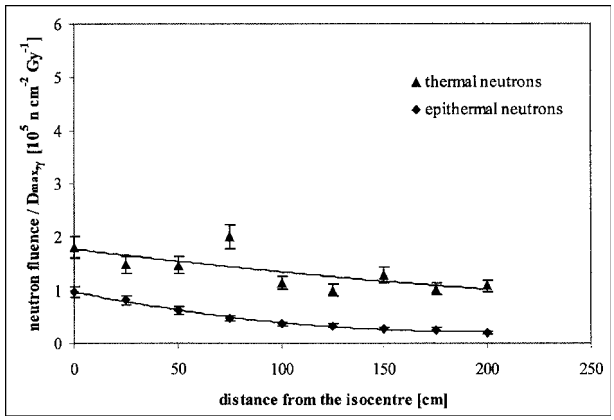

Fig. 6. The thermal and epithermal neutron fluence distributions along the axis x_2 for s = 6 cm × 6 cm specified at SSD = 60 cm.

6 cm × 6 cm radiation field specified at SSD = 60 cm (Fig. 6 and Tables 1 and 2). In these measurements, the indium foil detectors were placed on the surface of the treatment couch.

The distributions of the thermal and epithermal neutron fluences along the axes x_3 and y_3 (plane C) are presented in Figs. 7 and 8, respectively. The indium foil detectors were placed on a thin cardboard attached to the wedge mount.

The thermal and epithermal neutron distribution measured on the front of the accelerator head casing (plane D) is presented in Fig. 9.

Results for the electron beams of 18 MeV and 21 MeV

Measurements of the thermal and epithermal neutrons during the emission of electron beams were only performed at the isocentre for a radiation field of 10 cm × 10 cm specified at SSD = 100 cm. The obtained neutron fluence values were compared with that for the

Table 1. The thermal neutron fluence values in n · cm^{-2} · Gy^{-1} on axes y_1 and y_2

Location	Thermal neutron fluence, n · cm^{-2} · Gy^{-1}			
	5 cm × 5 cm at SSD = 100 cm	10 cm × 10 cm at SSD = 100 cm	20 cm × 20 cm at SSD = 100 cm	6 cm × 6 cm at SSD = 60 cm
–20 cm	3.5×10^5	2.0×10^5	2.7×10^5	1.2×10^5
0	3.9×10^5	3.0×10^5	2.7×10^5	1.1×10^5
20 cm	3.1×10^5	3.1×10^5	2.8×10^5	1.1×10^5

Table 2. The epithermal neutron fluence values in n · cm^{-2} · Gy^{-1} on axes y_1 and y_2

Location	Epithermal neutron fluence, n · cm^{-2} · Gy^{-1}			
	5 cm × 5 cm at SSD = 100 cm	10 cm × 10 cm at SSD = 100 cm	20 cm × 20 cm at SSD = 100 cm	6 cm × 6 cm at SSD = 60 cm
–20 cm	0.8×10^5	1.0×10^5	0.7×10^5	0.3×10^5
0	0.9×10^5	0.9×10^5	0.8×10^5	0.3×10^5
20 cm	0.9×10^5	0.9×10^5	0.7×10^5	0.4×10^5

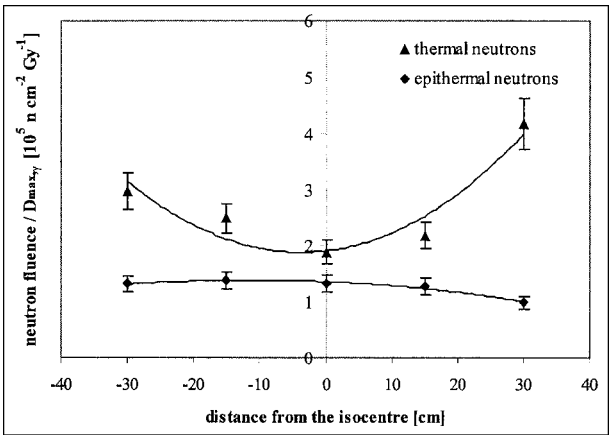

Fig. 7. The thermal and epithermal neutron fluence distributions along the axis x_3 for s = 10 cm × 10 cm specified at SSD = 100 cm.

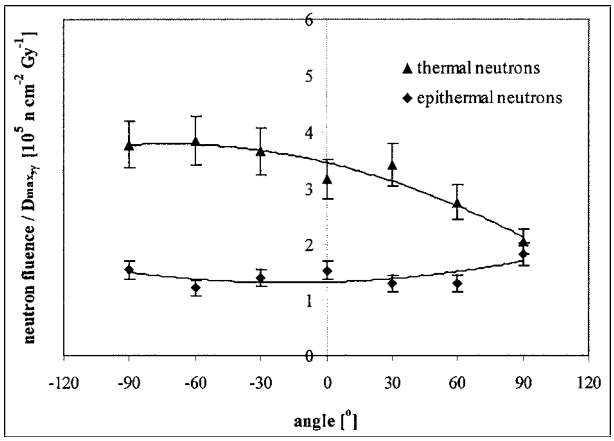

Fig. 9. The thermal and epithermal neutron fluence distributions on the front of the accelerator head casing (plane D) for s = 10 cm × 10 cm specified at SSD = 100 cm.

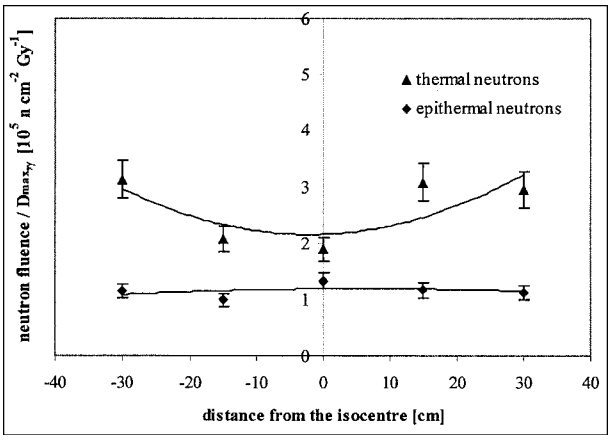

Fig. 8. The thermal and epithermal neutron fluence distributions along the axis y_3 for s = 10 cm × 10 cm specified at SSD = 100 cm.

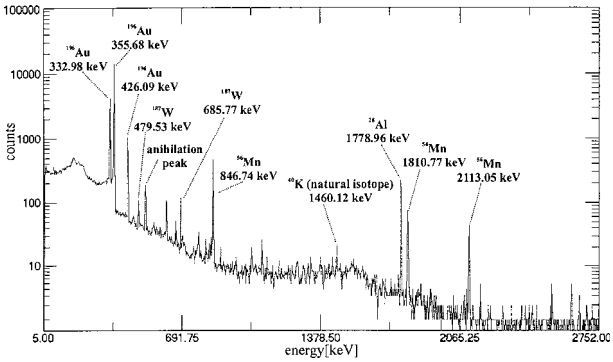

Fig. 10. The gamma energy spectrum measured under the accelerator head, at 30 cm from the wedge mount. The measurements was performed after the 15 MV beam emission lasting 15 min and the ventilation of the treatment room. The live time of the measurement was 115 seconds.

15 MV X-rays and three beams from Varian Clinac 2300 machine [11] (Table 3).

Measurements of gamma energy spectrum in the treatment room during a pause between beam emissions

The measurements were performed under the accelerator head after ventilating the treatment room. The obtained gamma energy spectrum is presented in Fig. 10. The ventilation makes it possible to avoid recording gammas from the decays of the ^{13}N (half-life 10.1 min) and ^{15}O (half-life 2.1 min) radioisotopes originating from the photonuclear reactions in air. Problem of the air activation during the high-energy therapeutic beam emission is widely known. It was considered in many papers. Analysis of the obtained spectrum (Table 4) was based on the knowledge of the materials used in the Primus Siemens accelerator construction.

Table 3. Comparison of the thermal and epithermal neutron fluence values in n · cm^{-2} · Gy^{-1} at the isocentre inside six therapeutic beams emitted by the Primus Siemens and Varian Clinac 2300 accelerators

Beam	Accelerator	Φ_{ther}, n · cm^{-2} · Gy^{-1}	Φ_{epi}, n · cm^{-2} · Gy^{-1}
15 MV	Primus Siemens	2.9×10^5	1.3×10^5
20 MV	Clinac Varian 2300	1.3×10^6	1.0×10^6
18 MeV	Primus Siemens	1.2×10^4	0.6×10^4
21 MeV	Primus Siemens	2.0×10^4	0.8×10^4
18 MeV	Clinac Varian 2300	0.7×10^4	1.5×10^4
22 MeV	Clinac Varian 2300	1.1×10^4	2.1×10^4

Table 4. Identification of the peaks visible in the gamma energy spectrum presented in Fig. 10

Activated isotope	Reaction	Originated radioisotope (and its half-life)	Radioactive decay	Emitted gammas, keV	Results of the decay (stable nucleus)
$^{197}_{79}$Au	(e,n) (e,e',n) (γ,nγ)	$^{196}_{79}$Au (6.183 d)	β⁻ EC	426.09 332.98 355.68	$^{196}_{80}$Hg $^{196}_{79}$Pt
$^{186}_{74}$W	(n,γ)	$^{187}_{74}$W (23.72 h)	β⁻	479.53 685.77	$^{187}_{75}$Re
$^{55}_{25}$Mn	(n,γ)	$^{56}_{25}$Mn (2.56 h)	β⁻	846.74 1810.77 2113.05	$^{56}_{26}$Fe
$^{27}_{13}$Al	(n,γ)	$^{28}_{12}$Al (2.24 m)	β⁻	1778.96	$^{28}_{14}$Si

Discussion

Uncertainties in the determined thermal and epithermal neutron fluences

Uncertainties in all experimental quantities used in Eqs. (3) and (4) were taken into account in the calculations of the accuracy of the applied method, i.e. to estimate the uncertainties in Φ_{ther} and Φ_{epi}.

One of these quantities giving a significant contribution to the uncertainties in the neutron fluence is the measured indium foil detector activity. Uncertainties in A_{ther} and A_{epi} (5–7% in the case of 15 MV beam and about 15% in the case of electron beam) depend on the statistics of the measurements of foil activity affected by the efficiency of the Ge(Li) detector, the neutron fluence value and the number of the ^{115}In atoms in the foil, i.e. the size and the density of the foil d_m. The size and shape of the foil have to correspond to the size and shape of the calibration source to calibrate the Ge(Li) detector. The ^{60}Co calibration source in the shape of a circle with a radius of 0.75 cm was used in our measurements. The use of the larger foil improve the statistics of measurements of the foil activity and decrease the uncertainties in A_{ther} and A_{epi} because the foil activity is then greater. However, we were not in possession of the larger calibration source. Moreover, to avoid increasing the self-shielding effects within indium foil, we did not increase also the foil density d_m.

Other two significant factors affecting the uncertainties in Φ_{ther} and Φ_{epi} are the accuracy of the determination of the foil area S (6.7%) and the foil density d_m (6.5%). The uncertainties in t_n (< 0.1%), in t' (< 0.2%) and in other quantities used in Eqs. (3) and (4) can be neglected.

The uncertainties in Φ_{ther} and Φ_{epi} were calculated as root of the sum of squared uncertainties of all experimental quantities applied in Eqs. (3) and (4), to be 10.4–11.5% in the measurements connected with the 15 MV X-rays and 17.5% in the measurements for the electron beams. The worse accuracy of the induce activity method in the case of the therapeutic electron beams is caused by the worse statistics in the measurements of the indium foil detector activity, which is a result of the smaller neutron flux generated during the electron beam emission.

Neutrons connected with the 15 MV X-ray emission

The thermal neutron fluence is about 2 ÷ 6 times greater than the epithermal fluence at all measurement points except for two cases: the first at the intersection of the axes x_3 and y_3, the second at 90° on the front of the accelerator head casing (plane D). The quotient of Φ_{ther} and Φ_{epi} is 1.3 and 1.1 at the point O_3 in plane C and at 90° in plane D. The point O_3 is located on the central axis of the therapeutic beam directly under the accelerator head. Thus, the location is nearest the target – the first important source of neutrons [16]. It is worth emphasizing that, in general, the quotient of Φ_{ther} and Φ_{epi} increases even up to 5.8 as the distance from the central axis of the therapeutic beam increases.

The singularity of the neutron fluence distribution for the angles over 30° in plane D is caused by the water cooling system located on the left-hand side of the accelerator head. The water cooling system is the only major part asymmetric to the central axis of the therapeutic beam in the head of the Primus Siemens accelerator.

The thermal neutron fluences vary between 1.1×10^5 n · cm^{-2} · Gy^{-1} and 4.4×10^5 n · cm^{-2} · Gy^{-1}. The greatest thermal neutron fluence was measured at 75 cm from the isocentre on the axis x_1 for s = 5 cm × 5 cm and at 30 cm on the axis x_3. There were not significant differences between the thermal neutron fluence values in plane A for s = 5 cm × 5 cm, 10 cm × 10 cm and 20 cm × 20 cm. The least thermal neutron fluences were measured in plane B. They did not exceed 2.0×10^5 n · cm^{-2} · Gy^{-1}. The difference in neutron fluence values for various radiation field is caused mainly by the normalization procedure, for example, averaged values of $\Phi_{ther,10\times10}/\Phi_{ther,6\times6} = 2.2$ and $\Phi_{epi,10\times10}/\Phi_{epi,6\times6} = 2.1$ whereas $D_{\max,\gamma,6\times6}/D_{\max,\gamma,10\times10} = 2.7$. The epithermal neutron fluences vary between 0.2×10^5 n · cm^{-2} · Gy^{-1} and 1.8×10^5 n · cm^{-2} · Gy^{-1}. The greatest epithermal neutron fluences were measured in plane D, whereas the smallest ones in planes A and B. In the case of epithermal neutrons the differences between neutron

fluence values for various radiation field were also due to the normalization procedure. In planes A and B, the epithermal neutron fluences decreases with increasing distance from the isocentre. This effect appears probably as a result of slowing-down neutrons in air.

The square function depicts the thermal and epithermal neutron fluence distributions quite well. Exceptions are the distributions of the thermal neutron fluences along the axes x_1, x_2 and y_3 and of the epithermal neutron fluences along y_3 and in plane D where several fluence values wander from the fitted curve. This heterogeneity in the neutron fluence distributions along x_1 and x_2 is probably caused by the structure of the treatment couch on which the indium foil detectors were located. The treatment couch consists of several parts differing in size and material. This is the reason of differences in absorption and scattering of neutrons passing through the treatment couch. This effect is visible particularly in the case of neutrons with thermal energy because the table-top is relatively thin and made of a low atomic number materials.

Neutrons connected with the electron beam emission

The thermal as well as epithermal neutron fluences at isocentre for the electron beam of 21 MeV were greater than for the electrons of 18 MeV. The thermal neutron fluence measured inside the electron beams of 18 MeV and 21 MeV emitted by the Primus Siemens machines is about two times greater than that for the 18 MeV and 22 MeV electron beams from the Varian Clinac 2300 machine, respectively. On the contrary, the epithermal neutron fluence for the Primus Siemens accelerator is almost three times lower than that for the Varian Clinac 2300. This is caused by the differences in construction of the accelerator head and in materials of the target, collimators and scattering foils [8]. The thermal as well as epithermal neutron fluences for the electron beams used in this work are about one order of magnitude lower than fluences measured inside the 15 MV X-rays and about two orders of magnitude lower than fluences inside the X-ray beam of 20 MV generated by the Varian Clinac 2300 machine. This fact was explained above.

The differences in fluence between the X-ray beams of 15 MV and 20 MV are caused by the fact that the maximum of the energy spectrum of the beam with higher nominal accelerating potential is closer to the resonance peak of the photonuclear reactions for the high atomic number materials, the major parts of the accelerator head are made of.

Consequences of the thermal and epithermal neutron production

In the treatment room, the radioisotopes resulting mainly from two kinds of reactions, i.e. photonuclear and simple capture reactions. However, the photon flux decreases strongly outside the therapeutic beam. Thus, the photonuclear reactions take place mainly in the accelerator head whereas the neutron flux does not change significantly even at 2 meters from the isocentre, and so the activation of the wall is induced by neutrons.

Electronuclear reactions are significant only in the target because of the very strong electron flux there. Reactions induced by protons and other charged particles are, of course, of the lowest importance because of the coulomb barrier of the nuclei.

The gamma spectrum measured under the accelerator head consists of two components, i.e. of the continuous spectrum and the peaks (Fig. 10). The continuous spectrum results mainly from the scaterred photons of the radioisotopes originating during the therapeutic beam emission. The cosmic rays and the scattered radiation of natural radioisotopes does not give a significant contribution to the continuous spectrum as the measurements of backgrounds showed (not presented in this paper), which were carried out in the treatment room two days after beam emission and in some others rooms. The analysis of the shown spectrum was carried out on the ground of knowledge of the materials used in the Primus Siemens accelerator construction.

The first three peaks at 332.98 keV, 355.68 keV and 462.09 keV (Fig. 10) are a result of the decay of the ^{196}Au nuclei (half-life 6.183 d) originating from the electronuclear reactions ^{197}Au(e,n)^{196}Au and ^{197}Au(e,e'nγ)^{196}Au and the photonuclear reaction ^{197}Au(γ,nγ)^{196}Au [5] taking place in the target – the only part of the Primus Siemens made of gold. In spite of the high cross section of the simple capture reaction ^{197}Au(n,γ)^{198}Au (the thermal neutron simple capture cross section of 96 barns and resonance activation integral of 1558 barns) [20] the gammas (411.8 keV) from the decays of ^{197}Au are absent in the presented spectrum because the fast neutrons originate in the target and the neutrons leave it before they reach the thermal and resonance energies.

The major massive parts of the Primus Siemens head, i.e. the primary collimator and jaws are made of tungsten. There are four natural stable isotopes of tungsten: ^{182}W, ^{183}W, ^{184}W and ^{186}W which can be activated by thermal neutrons as well as the epithermal ones. However, the neutron activaction of the ^{182}W and ^{183}W isotopes gives stable isotopes without any metastable states. The observed peaks at 479.53 keV and 685.77 keV come from the decay of the ^{187}W nuclei (half-life 23.72 h) originating from the reaction ^{186}W(n,γ)^{187}W [5]. As a result of the n + ^{184}W reaction, two unstable states with the long half-lives originate: ^{185m}W (half-life 1.67 m, deexciting by gammas), ^{185}W (half-life 75.1 d, betas and gammas emitted). However, peaks from the decays of these two states are not visible in the presented spectrum because the energies of the emitted gammas do not exceed 132 keV and they are covered by the low-energy part of the continuous spectrum. They are observed in the spectrum (not presented in this paper) measured in the vicinity of the accelerator head after a several-day-long interruption in the beam emission.

The peaks at 1810.77 keV and 2113.05 keV come from the decays of the ^{56}Mn nuclei (half-life 2.56 h) originating from the reaction ^{55}Mn(n,γ)^{56}Mn [5]. Manganese is one of the main components of stainless steel flattening filter, wedges and some smaller parts of the Primus Siemens machine. ^{55}Mn (stable) is the only

natural isotope of manganese. This isotope is easily activated by neutrons because it has a large cross section for the simple capture (the thermal neutron simple capture cross section of 13.2 barns and resonance activation integral of 15.7 barns, high resonance peak at 337 eV) [20].

Moreover, the peak at 1778.96 keV with a relatively high intensity is visible in the presented spectrum. It comes from the decay of the ^{28}Al isotope originating from the thermal and epithernal neutron activation of ^{27}Al [5] (the only natural isotope of aluminium). The existence of this peak is justified because three aluminium parts of the Primus Siemens head are used in the mode of 15 MV beam emission, i.e. the absorber inside the primary collimator (under the target), dose chamber and wedge tray and two other aluminium parts: secondary foil and applicator body are used in the mode of the electron beam emission.

Conclusion

Many investigations on the problems associated with neutron production from biomedical accelerators and the risk for personnel have been made during the last twenty years [4, 9, and others]. There is a renewed interest in these problems during the last few years [7, 22, and others] due to the increased use of high energy accelerators with high dose rates. Problem of the neutron activation of the accelerator parts and objects locating in the treatment room seems to be very important because the personnel (technicians) operating the accelerator, locating patients on the treatment couch etc. spend a lot of time in the vicinity of the accelerator. In this paper, the neutron fluence distributions and the gamma energy spectrum in the vicinity of the accelerator head were measured. This place of the measurement correspond to the frequent location of a technician. We measured also the gamma energy spectra in other places, but they are not presented in this paper. They were useful for the analysis of the shown spectrum.

We did not estimate the doses to personnel because the dose values depend on some changeable factors. First of all, they depend on the time of the therapeutic beam emission, especially, of the 15 MV beam emission and on the time of pause between the patient irradiations. The activities performing by the personnel in the treatment room are also important. For example, the technicians hold often the activated wedges in their hands, putting the wedge on a wedge tray. The time of this activity influences the dose value. Thus, the appropriate cours of the work and the sequence of the emitted beam, avoiding the longer emission of the 15 MV beam etc. can reduce the radiation level in the vicinity of the accelerator head. The widely-known problem of the air activation was passed over in this paper. However, it is worth stressing that the radioisotope originating in air can be successfuly removed by the continuous ventilation of the treatment room.

References

1. Beckurc K, Wirtc K (eds) (1968) Nejtronnaya fizika. Atomizdat, Moskva
2. Berman BL, Dietrich SS (eds) (1998) Atlas of photonuclear cross sections obtained with monoenergetic photons. Atom Data Nucl Data 38;2:199–338
3. Carrier J-F, Archambault L, Beaulieu L (2004) Validation of GEANT4, an object-oriented Monte Carlo toolkit, for simulations in medical physics. Med Phys 31;3:484–492
4. Cymermam U, Majenka A (1984) Determination of the doses of the photon and neutron secondary radiation from the Saturne-20 linear accelerator. Nowotwory 34;1:31–37 (in Polish)
5. Firestone RB (eds) (1996) Table of isotopes, 8th ed., version 1.0. Lawrence Berkeley National Laboratory, University of California
6. Firk FWK (1970) Low-energy photonuclear reactions. Annu Rev Nucl Sci 20:39
7. Followill DS, Stovall MS, Kry SF, Ibbatt GS (2003) Neutron source strength measurements for Varian, Siemens, Elekta and General Electric linear accelerator. J Appl Clin Med Phys 4;3:189–194
8. Gudowska J, Brahme A (1996) Neutron radiation from high-energy X-ray medical accelerators. Nukleonika 41;2:105–118
9. ICRP (1995) Conversion coefficient for use in radiological protection against external radiation. ICRP Publication 74
10. Kase KR, Mao XS, Nelson WR, Liu JC, Kleck JH, Elsalim M (1998) Neutron fluence and energy spectra around the Varian Clinac 2100/2300C medical accelerator. Health Phys 74;1:38–47
11. Konefał A, Orlef A, Zipper W, Dorda J, Łobodziec W (2001) Undesired neutron radiation generated by biomedical accelerators during high-energy X-ray and electron beam emission. Pol J Med Phys Eng 2;7(4):291–304
12. Konefał A, Orlef A, Zipper W, Maniakowski Z (2003) The use of the new Monte Carlo software packet called GEANT4 for the calculations of the doses from the X-rays outside the primary beam. Phys Med 20;S1:s147–s149
13. Levinger JS (1960) Nuclear photo disintegration. Oxford University Press, London
14. MacDonald N (ed.) (1965) Nuclear structure and electromagnetic interaction. Plenum, New York
15. Macklin RL, Pomerance HS (1956) Neutron cross sections. In: Proc of the Int Conf on the Peaceful Uses of Atomic Energy. Vol. 5. United Nations, New York, p 96
16. Mao XS, Kase KR, Liu JC, Nelson WR, Kleck JH, Johnsen S (1997) Neutron source in the Varian Clinac 2100/2300 medical accelerator calculated by the EGS4 code. Health Phys 72;4:524–529
17. National Bureau of Standards (NBS) (1973) Photonuclear reaction data. NBS Special Publication 380, Washington, D C
18. National Bureau of Standards (NBS) (1982) Photonuclear Data Index. NBSIR 82-2543, Washington, D C
19. Ongaro C, Zanini A, Natashi U, Rodenas J, Ottaviano G, Manfredatti C (2000) Analysis of photoneutron spectra produced in medical accelerators. Phys Med Biol 45:L55–L61
20. Price WJ (1964) Nuclear radiation detection. McGraw-Hill Book Co., USA
21. Scott MB, Hanson AO, Kerst DW (1955) Electro- and photo-disintegration cross sections of ^{63}Cu. Phys Rev 100:205
22. Wu RK, McGinley PH (2003) Neutron and capture gamma along maze of linear accelerator vaults. J Appl Clin Med Phys 4;2:162–171